Eur Biophys J (1999) 28: 91–101

ARTICLE

Martin Oheim · Dinah Loerke · Walter Stühmer
Robert H. Chow

Multiple stimulation-dependent processes regulate the size of the releasable pool of vesicles

Received: 10 August 1998 / Revised version: 24 September 1998 / Accepted: 24 September 1998

Abstract In neuroendocrine cells and neurones, changes in the size of a limited pool of readily releasable vesicles contribute to the plasticity of secretion. We have studied the dynamic alterations in the size of a near-membrane pool of vesicles in living neuroendocrine cells. Using evanescent wave microscopy we monitored the behaviour of individual secretory vesicles at the plasma membrane. Vesicles undergo sequential transitions between several states of differing fluorescence intensity and mobility. The transitions are reversible, except for the fusion step, and even in nonstimulated conditions the vesicles change states in a dynamic equilibrium. Stimulation selectively speeds up the three forward transitions leading towards exocytosis. Vesicles lose mobility in all three dimensions upon approach of the plasma membrane. Their movement is directed and targeted to the docking fusion sites. Sites of vesicle docking and exocytosis are distributed non-uniformly over the studied "footprint" region of the cell. While some areas are the sites of repeated vesicle docking and fusion, others are completely devoid of spots. Vesicular mobility at the membrane is confined, as if the vesicle were imprisoned in a cage or tethered to a binding site.

Key words Total internal reflection · Evanescent wave microscopy · Optical sectioning · Ca^{2+}-triggered exocytosis · Vesicle fusion

M. Oheim · D. Loerke · W. Stühmer
Max-Planck Institute for Experimental Medicine,
Department of Molecular Biology of Neuronal Signals,
Hermann-Rein Strasse 3, D-37075 Göttingen, Germany

M. Oheim · R. H. Chow (✉)
Department of Biomedical Sciences,
University of Edinburgh Medical School,
Membrane Biology Group,
Teviot Place, Edinburgh EH8 9AG, Scotland
e-mail: robert.chow@ed.ac.uk

Introduction

The release-ready pool of vesicles

A common feature of many secretory cells is that the rate of exocytosis declines precipitously upon repeated or maintained stimulation (for work on neurones, see Elmqvist and Quastel 1965; Betz 1970; Stevens and Tsujimoto 1995; Rosenmund and Stevens 1996; for work on neuroendocrine cells, see Bittner and Holz 1992; Ammala et al. 1993; Gillis and Misler 1993; Horrigan and Bookman 1994; Parsons et al. 1995; Gillis and Chow 1997). After a pause in stimulation, the rate of exocytosis recovers. This has been interpreted to be due to depletion of a finite "readily releasable" pool of secretory vesicles, and then, upon cessation of the stimulus, replenishment of this pool from another, "reserve" pool. Until recently, the dynamics of individual vesicles in these functional pools, located at or near the plasma membrane, were hidden to the experimenter, since standard assays for secretion gave only indirect information about vesicle states prior to exocytosis, or did not offer sufficient resolution.

Evanescent-wave microscopy

The introduction of evanescent wave microscopy to studies of exocytosis (Steyer et al. 1997; Oheim et al. 1998) has made possible the direct observation of individual dye-loaded dense-core vesicles prior to exocytosis in living neuroendocrine cells. Light incident on a dielectric interface (from a higher to a lower refractive index medium) is totally reflected back into the higher refractive index medium if the angle of incidence exceeds the critical angle for total reflection. An exponentially decaying evanescent field is created in the lower index medium. The exponential decay constant of the evanescent field intensity is typically 70–300 nm. Its precise value depends on media refractive indices, incidence angle and illumination wavelength. Additionally, the evanescent field intensity depends on the polarisation angle of the incident light.

In this study, we analysed the trajectories of single fluorescently labelled dense-core vesicles as they approached the plasma membrane at the base of a cell illuminated by an evanescent field until they underwent exocytosis. We identified different functional states of the vesicles and examined how stimulating secretion affects the rates of exchange among these states.

Theory

Total internal reflection

The evanescent field generated by total internal reflection (TIR) illumination at a dielectric interface penetrates into the medium of lower refractive index. The evanescent field intensity decays exponentially with distance z from the interface

$$I(z) = I(0) \exp(-z/d) \quad (1)$$

where decay length

$$d = \frac{\lambda_0}{4\pi \sqrt{n_1^2 \sin^2 \theta_i - n_2^2}} \quad (2)$$

is a function of the refractive indices, n_1 and n_2, respectively, the angle of incidence θ_i and the wavelength. The intensity of the evanescent wave field at the interface, $I(0)$, is calculated by coherent superposition of the incident and reflected beam and solving Maxwell's equations for the appropriate boundary conditions. It depends on the angle of incidence, the refractive indices and the electric field amplitude A of the incident wave (Born and Wolf 1980). For s-polarised light

$$I_s(0) = |A_s|^2 \, 4\cos^2 \theta_i / (1 - n_2^2 / n_1^2) \quad (3)$$

and

$$I_p(0) = |A_p|^2 \, \frac{4\cos^2 \theta_i (2\sin^2 \theta_i - n_2^2 / n_1^2)}{(n_2 / n_1)^4 \cos^2 \theta_i + \sin^2 \theta_i - n_2^2 / n_1^2} \quad (4)$$

for p-polarised light. Evanescent (decaying) waves carry no net energy flux. However, energy can be transferred from the evanescent field if absorbing chromophores are present (a phenomenon called "frustrated" or attenuated TIR). The absorbed energy can be dissipated non-radiatively, or – if the chromophore has a non-zero quantum yield – by fluorescence emission.

Owing to the exponential decay of the evanescent field, TIR fluorescence microscopy (TIRFM) achieves its highest sensitivity very close to a dielectric interface. Thus, it lends itself in a natural way to investigations of surface topography, film thickness, refractive index and absorption close to interfaces. Throughout this study, evanescent waves were used to excite near-membrane fluorophores in cells grown on coverslips. The boundary between the aqueous cytosol and glass substrate constitutes the reflecting interface.

Materials and methods

Details of cell preparation, staining and the evanescent-wave set-up were as previously described (Oheim et al. 1998). Modifications of the optical system included a 16-bit CCD imaging system (Penta-Max, Princeton Instruments, Trenton, N. J., USA) equipped with a GenIV image intensifier and an acousto-optical deflector in the excitation light path to introduce fast reproducible variations of the angle of incidence.

Visualisation of individual vesicles in living cells

Bovine adrenal chromaffin cells were prepared as described elsewhere (Zhou and Neher 1993) and used on days 2–3 after preparation. Vesicles were stained with acridine orange (3 min incubation in a solution containing 2 μM dye, 145 mM NaCl, 10 mM HEPES, (pH 7.2), 2.8 mM $MgCl_2$, 2 mM $CaCl_2$ and 5 μM dye). The extracellular solution to trigger secretion was composed of 60 mM KCl, 85 mM NaCl, 10 mM HEPES (pH 7.2), 2.8 mM $MgCl_2$ and 2 mM $CaCl_2$. All experiments were done at 20–22 °C.

Evanescent-wave excitation

Fluorescence microscopy was performed using a custom-made TIR microscope based on a Zeiss Axioskop upright microscope (see Oheim et al. 1998 for a detailed description). The incidence angle θ_i was measured from the normal to the prism's planar surface to the beam's central axis. The calculated critical angle was (61.97 ± 1.2)°, assuming values of n_2 = 1.33–1.36 for the cytoplasm and n_1 = 1.52 (24) (at λ = 488 nm) for BK-7 glass. Owing to the uncertainty in n_2, $\theta_{i,c}$ was determined experimentally by increasing θ_i until TIR was observed. The decay length d was measured as described previously (Oheim et al. 1998), and found to range between 70 nm and 128 nm for incidence angles between 71.5° and 64°. Vesicles become visible as they enter the evanescent field. The total number of visible vesicles is thus dependent on the angle of beam incidence.

Telecentric optics allows a simple beam scan

Variations of the beam incidence were attained with an acousto-optic device (AOD) (Laser 2000, Wessling, Germany) and telecentric optics (Fig. 1). In usual scanning devices, a beam emerges from a fixed point at different angles and is scanned over the object. For TIRF experiments, a geometry is desirable in which the location at which the laser beam is aimed is kept fixed while the incidence angle is varied systematically. This was accomplished by a system of two convex lenses. The exit pupil of the AOD is placed in the back focal plane of the first lens (achromate f_1 = 15 cm) such that the angular scan is converted to a parallel displacement of the beam. This displacement is con-

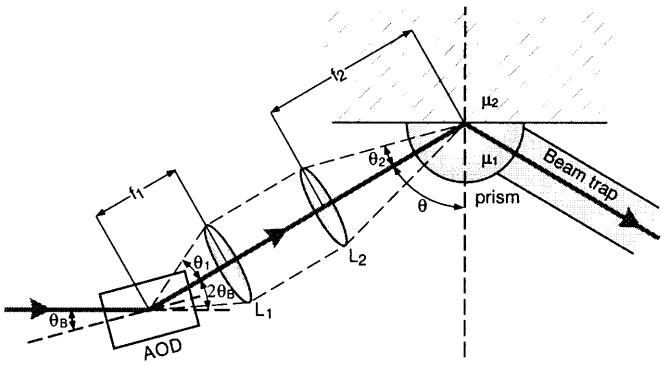

Fig. 1 Schematic of the telecentric optics used to keep the point of beam incidence fixed while varying the beam angle. A relay lens (L_1) transforms the scan angle into a parallel beam displacement. The focusing lens (L_2, at an arbitrary distance relative to of the first lens) ensures that the beam converges to the midpoint of the hemicylindrical lens, irrespective of the incidence angle. Fast reproducible variations of the scan angle are introduced by an acousto-optic deflector (*AOD*). The ratio of the two lenses can be used to magnify the scan angle to yield the desired angle of incidence at the reflecting interface. An index-matched glass-rod is optically coupled to the cylindrical lens to guide the reflected beam to a beam trap and avoid scattering and reflection at the surface as the beam leaves the prism

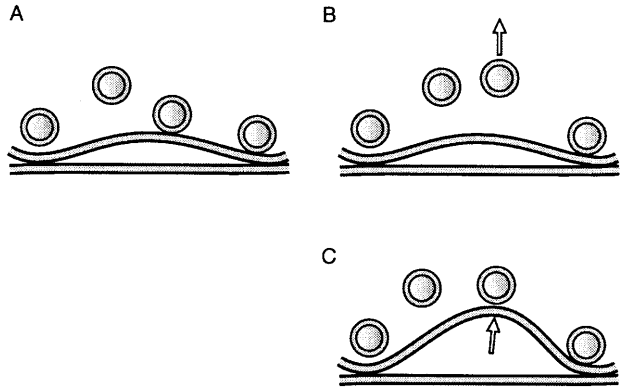

Fig. 2 A–C Complications in the interpretation of evanescent-wave fluorescence images. Total internal reflection occurs at the top of the glass coverslip (n = 1.5224), irrespective of the precise refractive index of the low index medium. Changes in fluorescence represent distance changes with respect to the reflecting interface **A**. A decrease in fluorescence intensity of a vesicle could be due to **B** withdrawal of the vesicle from the membrane or else **C** buckling up of the membrane with the vesicle at the same membrane/vesicle separation distance. Thus, dynamic alterations of the cell/substrate contact region that can occur during experiments, particularly after long observation periods, solution exchange or whole-cell dialysis result in changes in the evanescent-wave fluorescence images that are hard to interpret

verted back to a change in beam incidence by placing the focus of the second achromate (f_2 = 6 cm) such that it coincides with the point at the dielectric interface at which TIR occurs. The ratio of focal lengths determines the final scan angle, 4.8°

$$\theta_2 = \tan^{-1}(\theta_1 \cdot (f_1/f_2)) \quad (5)$$

Guiding the beam to the reflecting interface

A hemicylindrical BK-7 (n = 1.5224) prism of 5.5 mm radius (Spindler & Hoyer, Göttingen, Germany) guided the incident beam without refraction to the same location on the stage of an upright microscope (Zeiss Axioskop, Jena, Germany), irrespective of the angle of incidence. The prism was cut and optically polished such that the midpoint of symmetry was at the upper surface of a coverslip of 0.17 mm thickness when coupled to the prism's planar surface by a thin layer of immersion oil. To arrive at a reproducible thickness of the oil film, 3 μl of oil were applied to the prism's top with a micro pipette. A 4-mm diameter BK-7 glass rod (custom-made in the optics workshop, MPI for Biophysical Chemistry, Göttingen, Germany) was optically coupled to the rounded site of the hemicylindrical prism with immersion oil, allowing the reflected beam to leave the prism without significant reflection back to the flat top. The end of the rod was cut at an angle of 45° and mantled with black matte plasticine such that it acted as a beam trap.

Image acquisition

Images where acquired with an intensified frame-transfer CCD camera (Princeton Instruments, Trenton, N. J., USA) with a maximum quantum efficiency of 35% at 550 nm. Acquisition, storage and analysis were performed using MetaMorph (Universal Imaging, West Chester, Pa., USA). Full images were typically recorded every 200 ms (5 Hz); images of sub-regions were taken at up to 200 Hz.

Ambiguities in the interpretation of fluorescence data

Penetration depths of the evanescent wave were determined as previously described by measuring the fluorescence signal of a bead attached to the tip of a glass pipette at distances from the reflecting interface (Oheim et al. 1998). However, the knowledge of the penetration depth of the evanescent wave into the aqueous solution on top of the coverslip does not allow an unequivocal interpretation of fluorescence intensities (see Fig. 2): vesicles of equal brightness are not necessarily located at equal distances from the plasma membrane, because:

1. The plane of reference for evanescent-wave distance measurements is the glass/water interface – at which the light is reflected – rather than the plasma membrane.
2. The value of the decay-length of the evanescent wave, determined in aqueous solution, is modified by the higher-refractive index medium of the cytoplasm.

Image analysis

The ambiguity in the interpretation of fluorescence intensity makes it difficult to obtain a knowledge of the func-

tional states of vesicles prior to fusion without further data. Additional information comes from particle mobility. Particle tracking first requires incubation of the cell with fluorescent dye to visualise vesicles as individual pinpoints (Steyer et al. 1997; Oheim et al. 1998). Cells with low vesicle densities and small penetration depth facilitate this task. The images were digitised, stored and later analysed in an image processor running the MetaMorph software package (Universal Imaging, West Chester, Pa., USA). A macro recognises, locates and tracks the individual fluorescently labelled vesicles from image to image and consequently yields the precise trajectories.

Single-vesicle tracking in three-dimensional space

The automated tracking of vesicle positions involved the iterative application of two steps: the first identified the search object and an extended search region in the current image, and the second one matched the objects found in the next image with those identified in the current image. If an object was lost, the algorithm first looked one plane ahead, then expanded the search region and finally switched to the interactive mode. The (lateral) position of particle $(\hat{x}, \hat{y})$ was defined as the weighted "centre of mass" of its image over the pixels it covered

$$\hat{x} = \frac{\sum_{x,y} x(\tilde{F}(x,y) - F_T)}{\sum_{x,y} (\tilde{F}(x,y) - F_T)}, \quad \hat{y} = \frac{\sum_{x,y} y(\tilde{F}(x,y) - F_T)}{\sum_{x,y} (\tilde{F}(x,y) - F_T)} \tag{6}$$

where $\tilde{F}$ is the fluorescence intensity and F_T is a threshold to eliminate fluctuations in the background. This procedure resembles the introduction of centre-of-mass co-ordinates in classical mechanics and is repeated for each individual vesicle and image plane.

"Local" co-ordinates

Evanescent wave microscopy allows us to determine particle trajectories in three dimensions. However, non-linear filtering that is usually employed prior to identification of particle positions (Gosh and Webb 1994; Steyer et al. 1997) will not only remove intracellular background from the images and highlight particle positions but also change peak intensities. This brings about the need to develop an alternative tracking algorithm if 3-D positional information is desired. A way to relate fluorescence changes to distances travelled and to decide whether the entire membrane buckles up or the individual vesicle withdraws from the plasma membrane is to look at the intensity peaks and the local background changes at the same time. This corresponds to introducing a local co-ordinate system in which each vesicle is characterised by fitting a 2-D Gaussian distribution to the intensity distribution. Fit parameters include the peak position of the distribution, the maximum intensity F, the width of the distribution and the local background B. The change in axial position is calculated according to

$$z = -d \ln((F-B)/(F_0-B_0)) \tag{7}$$

where F_0 and B_0 are the peak fluorescence and background on the preceding image, and d is the penetration depth. After reading out fluorescence intensities, images can be thresholded to facilitate particle tracking in the lateral plane.

Calculation of the 3-D diffusion coefficient

The lateral displacement [Eq. (6)] and fluorescence F [Eq. (7)] were used to calculate a 3-D diffusion coefficient, $D^{(3)}$. Let δt the time between two consecutive images, $\Delta t_n = n \cdot \delta t$ (n integer), and $l(\Delta t_n)$ the distance that a vesicle travels in the time interval Δt_n. Then $\langle l^2(\Delta t_n)\rangle_n$ defines the mean squared displacement (MSD) in a time interval Δt_n:

$$\left\langle l^2(\Delta t_n)\right\rangle = \frac{1}{N-n} \sum_{j=1}^{3} \sum_{k=1}^{N-n} \left\{[x_j((k+n)\,\delta t) - x_j(k\,\delta t)]^2\right\} \tag{8}$$

where $\boldsymbol{r} = (x, y, z)$ is written as $(x_j)\big|_{j=1,\ldots,3}$; N is the total number of images. Thus, the MSD for δt measures how far, on average, a particle travelled in the time interval $[0, \delta t]$, MSD $(2\,\delta t)$ measures how far it travelled in $[0, 2\,\delta t]$, and so on. Plotting MSD versus Δt_n, the three-dimensional diffusion coefficient is given by the asymptote

$$D^{(3)} \equiv \frac{1}{6} \left.\frac{\mathrm{d}\left\langle l^2(\Delta t_n)\right\rangle_n}{d\Delta t_n}\right|_{\Delta t_n \to 0} \tag{9}$$

$D^{(3)}$ was determined from a linear fit to the first 3–5 points on a plot of MSD versus Δt_n. The intercept was forced to the origin. Individual points contributed as 1 over the standard deviation of the MSD; δt was 100 ms. This procedure defines an average "short-range diffusion coefficient". Vibrations of the stage, determined from stationary 100-nm fluorescent beads on the coverglass, limit the resolvable diffusion coefficient to $D^{(3)}_{\min} = 5.73 \pm 1.33\ 10^{-13}$ cm^2 s^{-1}. The value of $D^{(3)}$ over time was also taken as a control parameter of cell activity. A continuous decrease of $l(\Delta t_n)$ and thus $D^{(3)}$ for many vesicles with experiment time indicated a run-down of cellular activity, e.g. due to loss of ATP after whole-cell dialysis.

Results

Findings from non-stimulated cells

After preincubation of bovine chromaffin cells in acridine orange – an acidotropic fluorescent dye that accumulates in acidic vesicular compartments – TIR illumination of unstimulated cells revealed punctuate fluorescence in the adherent "footprint" of the cell (Fig. 3A).

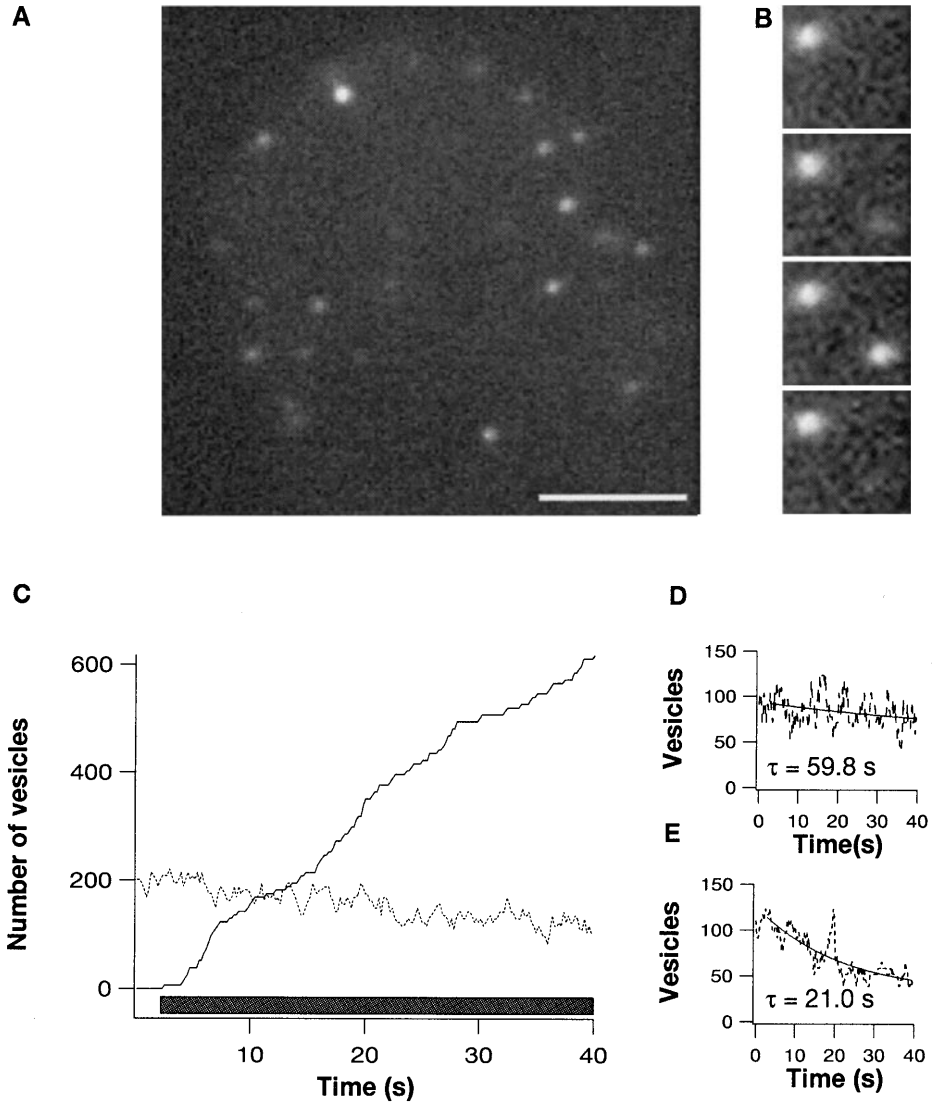

Fig. 3A–E Individual vesicles prior to exocytosis, observed with evanescent wave microscopy. Cells were incubated with acridine orange. The 200-ms images were taken with an intensified CCD camera. **A** Large dense-core vesicles are seen as fluorescent spots in the "footprint" region of a chromaffin cell. The footprint diameter is ≈14 μm (the *scalebar* indicates 5 μm). The angle of incidence was 70.0°, corresponding to a calculated penetration depth of the evanescent wave of 75 nm. **B** Vesicles enter and leave the region of excitation. About half of the vesicles are highly mobile, but exhibit diffusion restricted to a cage with diameter ≈300 nm. The other half has a mobility that is two orders of magnitude smaller, as if the vesicles were tethered to a binding site or imprisioned in a cage. Slow diffusion of the "cage" or binding site itself is barely resolvable and of the order of 6×10^{-13} cm^2 s^{-1}. **C** In resting cells, about 30–34 vesicles are visible within the footprint region, corresponding to an average density of 0.11 ± 0.3 μm^{-2}. The total number of visible vesicles decreases only gradually after stimulation, indicating a supply of new vesicles to the observed region. The *grey bar* indicates the timing of a local application of 60 mM K^+ from a puffer pipette. The *solid trace* represents the cumulative number of vesicles lost through exocytosis. Secretion starts at t = 2.6 s, 100 ms after K^+ application. **D** The number of highly mobile vesicles changes only after maintained stimulation and decays monoexponentially with a time constant of about 1 min. **E** The average number of less mobile vesicles decreases after stimulation with a time constant of about 20 s (n = 7 cells)

Vesicles display two levels of brightness

These spots, shown previously (Steyer et al. 1997; Oheim et al. 1998) to correspond to individual secretory vesicles, exhibited two levels of brightness. For a penetration depth of the evanescent field of 75 nm, the total number of near-membrane vesicles in the footprint region was 30 ± 4. This number represents the time-average of the number of spots in a time-series of images in the absence of stimulation. Spots were counted as vesicles if the average intensity in the central 3×3 pixel region exceeded five times the peak-to-peak noise of intracellular background on three consecutive frames. On average, 47% of the vesicles (14 ± 2 spots, see legend to Fig. 3C) had an intensity F of 23.3 ± 8.6 cts/pixel, and 53% (16 ± 2 spots) an average intensity of 42.0 ± 3.8 cts/pixel. If one assumes as a first approximation that the vesicles are distributed at uniform density over the entire cell membrane, and that the footprint of the cell represents approximately 15% of the total cell membrane surface area, then the total number of vesicles in the shell near the plasma membrane can be estimated to be about 200 in

resting cells, of which about 90 are dim and highly mobile while roughly 110 are brighter and less mobile.

Diffusion coefficients of mobile and immobile vesicles differ by two orders of magnitude

There were also two levels of vesicle mobility, analysed here in terms of the 3-D diffusion coefficient $D^{(3)}$. Interestingly, the level of mobility was inversely related to the fluorescence intensity, as shown in Fig. 4A. The diffusion coefficient of the dimmer, mobile class of vesicles was on average $3.23 \pm 0.92\ 10^{-10}$ cm^2 s^{-1} (mean ± SD, $N = 112$), whereas the bright vesicles were almost completely immobile with $D^{(3)} = 2.7 \pm 1.1\ 10^{-12}$ cm^2 s^{-1} ($N = 138$). Transitions between states – and thus values of F and $D^{(3)}$ – were observed (Fig. 4B) but were fast compared to the lifetimes of vesicles in the mobile and immobile state, respectively (see legend to Fig. 5).

Vesicles lose their mobility as they approach the plasma membrane

The trajectory of a single vesicle from the time of its appearance to its disappearance, due to exocytosis, is shown on a plot of $D^{(3)}$ versus F. The vesicle moved from the dimmer, high mobility class to the brighter, less mobile one (Fig. 4B) with several reversals in direction before it finally disappeared after release of its contents into the extracellular space.

In the absence of stimulation, a dynamic equilibrium keeps pool sizes constant

While the sizes of the two visible vesicle pools remained constant in the absence of stimulation, vesicles occasionally changed from the brighter, less mobile state to the dimmer, highly mobile state, and vice versa, at a rate of 1.5 s^{-1}. (Rates are reported here as the number of vesicles undergoing a stated transition per second over the entire footprint region. To arrive at a whole-cell estimate, these numbers are multiplied by a factor of 6–7.) In addition, new vesicles spontaneously appeared or visible vesicles disappeared at equal rates of 7.1 s^{-1}, indicating a continuous exchange between vesicles that are visible and others in an invisible reserve pool – located deeper in the cell, beyond the reach of the evanescent field. For convenience, we refer to the pools of vesicles as V_1, V_2, and I, for vesicles that are dim and highly mobile, bright but less mobile, and "invisible", respectively.

Results from stimulated cells

Upon exposure of chromaffin cells to an extracellular solution containing 60 mM potassium, the fluorescent spots disappeared in a cloud of released dye molecules (Steyer

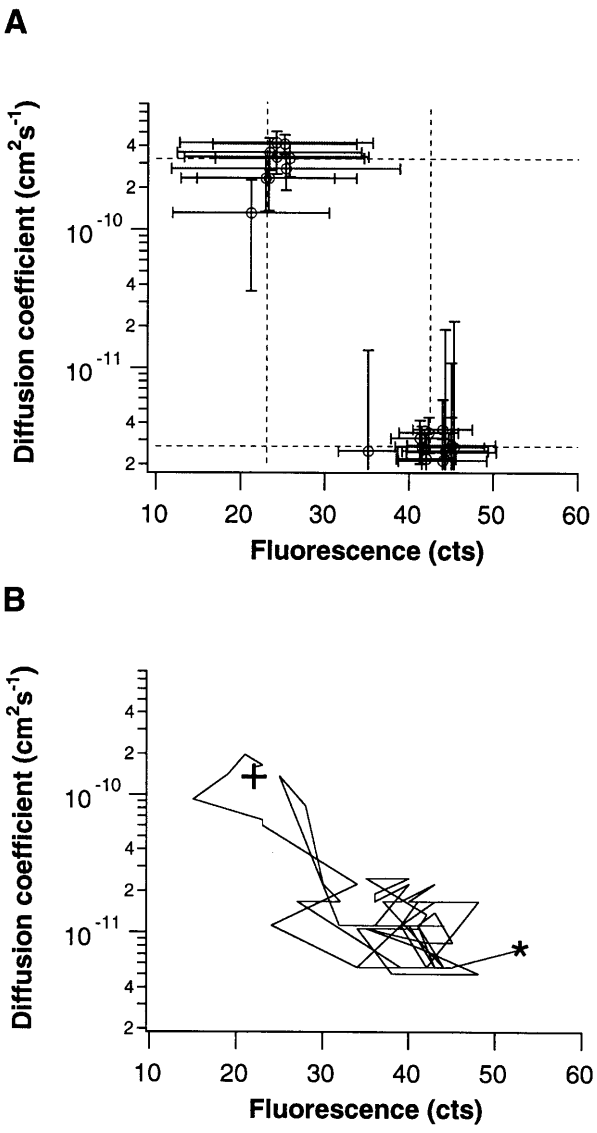

Fig. 4A, B Vesicles must go through different stages prior to fusion. **A** In resting and stimulated cells, each vesicle can be characterised based on its mobility and fluorescence intensity. The vesicles fall into two distinct groups: one group is mobile with an average three-dimensional diffusion coefficient $D^{(3)}$ of $3.23 \pm 0.92\ 10^{-10}$ cm^2 s^{-1} and an average fluorescence intensity of 23.3±8.6 cts. The other group is less mobile with an average $D^{(3)}$ of $2.7 \pm 1.1\ 10^{-12}$ cm^2 s^{-1} and an average intensity of 42.1±3.8 cts. The image acquisition rate was 5 Hz. Points ($D^{(3)}$, F) were determined for each vesicle individually from the slope of a plot of the mean squared displacement vs. time for $\Delta t \rightarrow 0$ and the mean fluorescence intensity in the same time interval. *Error bars* give standard deviations in $D^{(3)}$ and F. **B** An individual vesicle is traced from its entry into the evanescent field (*crosshair*) until it fuses with the plasma membrane (*star*). Fusion was detected as release of dye molecules and subsequent destaining of the spot. The vesicle is seen to undergo reversible transitions between the dim, highly mobile state and the brighter, less mobile state before fusing. The net "trajectory" illustrates that approaching the membrane goes along with a loss of mobility of almost two orders of magnitude when expressed in terms of the free diffusion coefficient $D^{(3)}$. This pattern was consitstently observed. Note the peak of intensity (*star*) as the dye is released in close proximity to the interface and efficiently excited by the evanescent wave

et al. 1997; Oheim et al. 1998). Spots that have disappeared will be referred to as vesicles accumulating in a pool E, for vesicles that have undergone exocytosis. In spite of the loss of vesicles, during the initial 15 s of maintained potassium elevation the total number of visible vesicles (pools $V_1 + V_2$) remained almost constant (Fig. 3C, dashed line). This was due to the recruitment of new vesicles from the invisible reserve pool I. Although the rate of recruitment of new vesicles was enhanced, the reverse rate remained constant.

Vesicle supply ultimately limits the rate of secretion

In the first 5 s after depolarisation, the supply of vesicles from I increased from 7.1 s^{-1} to 9.5 s^{-1}. After 20 s, the rate then decayed gradually to 6.8 s^{-1}. The rate of transition from V_1 to V_2 also increased, from 1.48 s to 1.88 s, within the first 5 s and reached its peak value at 5.5 s^{-1} within 8 s after stimulation. Eventually, the rate declined to 1.76 s^{-1}. The reverse rate remained constant at 1.49 s. The net effect of stimulation was that the pool of vesicles V_2 diminished first, while V_1 initially remained approximately stable in size. Ultimately, however, even this pool dwindled, as the rate of re-supply of vesicles from I declined and became rate limiting.

Immobilised vesicles do not necessarily fuse first

While no spontaneous fusion events were seen in the absence of stimulation, secretion became vigorous after membrane depolarisation. Somewhat surprisingly, the already docked bright vesicles did not necessarily fuse first. Instead, a large fraction of the immediate secretory response came from vesicles that had arrived only recently in the evanescent region and rapidly went through the sequence $I \rightarrow V_1 \rightarrow V_2 \rightarrow E$. Secretion continued after the end of the stimulus, often lasting hundreds of milliseconds. Frequently, several vesicles were seen to fuse sequentially in very confined regions of less than 1 μm diameter (see below).

A three-step model for secretion control in neuroendocrine cells

Vesicles acquire fusion competence by going through a sequence of transitions

Vesicles undergo a well-defined sequence of steps on the way to exocytosis. We summarise the sequence in a four-state kinetic diagram (Fig. 5A), with the previously named pools I, V_1, V_2 and E, and rate constants k_1, k_{-1}, k_2, k_{-2} and k_3 for the transitions between the pools. In the absence of stimulation, the rates of transition to and from each pool balance each other. Stimulation selectively enhances the forward rates by a transient increase of the forward rate constants (see legend to Fig. 5). The delay between the arrival of a vesicle in the pool V_2 and its fusion or withdrawal back into deeper regions of the cytoplasm was modulated by stimulation (see Fig. 5 and its legend). In resting cells, the average lifetime of a vesicle in V_2, calculated as one over the rate constants leading away from this state, $\tau(V_2) = 1/(k_{-2}+k_3)$, was about 40 s but scattered largely between a few seconds and more than a minute. $\tau(V_2)$ decreased upon stimulation to about 8 s before its value increased again for maintained or repetitive stimulation (see Fig. 5D). The average lifetime of vesicles in V_1, $\tau(V_1) = 1/(k_{-1}+k_2)$, was 3.5 s and was almost unaffected by stimulation (Fig. 5B, C).

Rare events

We never observed the reactions $I \rightarrow V_2$ and $V_1 \rightarrow E$, consistent with the view that fusion requires the sequential transitions as indicated in Fig. 3A. For two out of a total of 700 vesicles (<0.3%), we observed brief reversible transitions, $V_2 \leftrightarrow E$, before completed exocytosis, compatible with fast, reversible widening and narrowing of the fusion pore that are, however, not resolved in the present experiment (Breckenridge and Almers 1987; Albillos et al. 1997; Alvarez de Toledo et al. 1993). Convergence of two spots and the subsequent appearance of a single, larger spot was observed rarely (3/700, ≈0.4%) and could represent compound fusion (Alvarez de Toledo and Fernandez 1990). Less than 0.3% of the spots remained unchanged despite maintained stimulation. These could be vesicles trapped in the docked state V_2 or else non-secretory acidic compartments.

Spatial organisation of exocytosis in chromaffin cells

The sites of exocytosis were not uniformly distributed over the entire cellular footprint region. The rim and patchy areas in the centre were the sites of intense vesicle trafficking and exocytosis. As can be seen in Fig. 6, there was extensive overlap of the sites of successive vesicle fusions. Other areas had spots that did not undergo exocytosis despite stimulation or were devoid of spots (Fig. 6A, B). When dye was added to the extracellular fluid and allowed to diffuse beneath the cell (not shown), the footprint region remained dark – ruling out the possibility that areas devoid of vesicles were sites where the membrane had buckled up above the reach of the evanescent wave.

Discussion

Sequential transitions of vesicles prior to fusion

In the present paper, we have arrived at an operational definition of vesicle states, based on what can be resolved using evanescent wave microscopy. We have intentionally avoided using A, B and C to label the states, as these labels have been used in previous studies of functional ves-

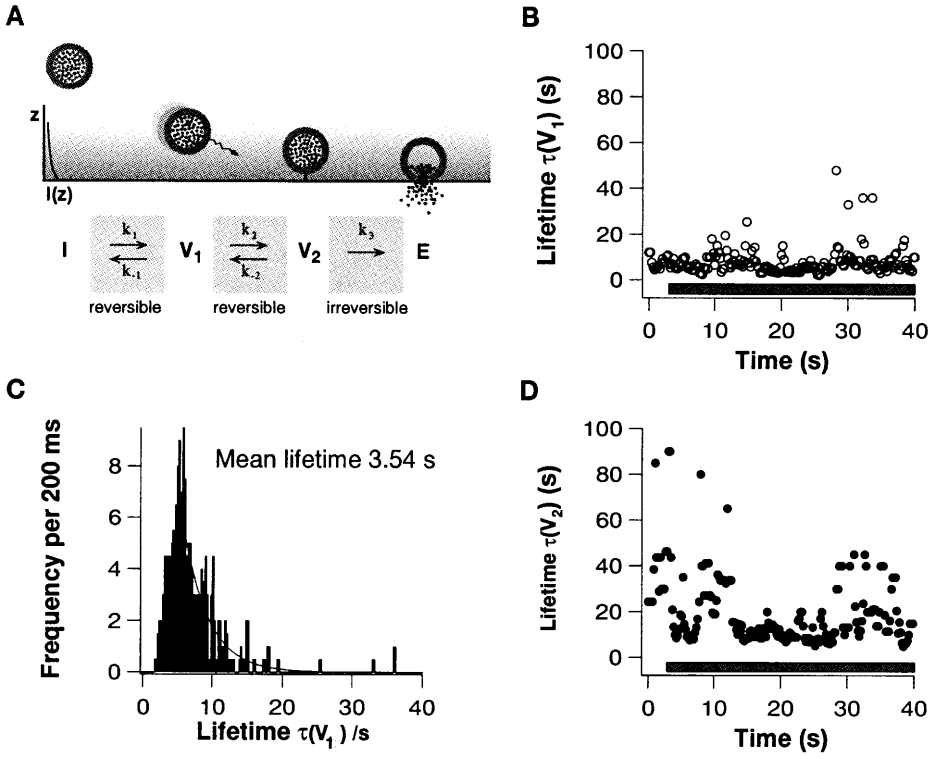

Fig. 5A–D A three-step sequential model of secretion control. **A** The bulk of the chromaffin granules is distant from evanescent excitation and therefore invisible in pool I. Vesicles approaching the membrane become visible when they enter the evanescent field in pool V_1, the vesicles of high-mobility and low-intensity. Upon approaching the plasma membrane they enter farther into the evanescent field, becoming brighter and simultaneously losing their mobility (pool V_2). The decrease in mobility may reflect molecular "docking" at the membrane. While progressing through these pools, vesicles probably undergo multiple biochemical maturation steps to become fully primed and ready for release (Parsons et al. 1995), but we cannot resolve these steps in the present experiment. Upon calcium triggering, vesicles in pool V_2 fuse to the membrane, joining pool E of exocytosed vesicles. Based on our observations, the steps between states I and V_1 and between V_1 and V_2 are reversible. Reversible steps from V_2 to E were not resolved. Rate constants were calculated by dividing the number of vesicles changing states between image frames by the pool size. Values were calculated as rolling averages to smooth out noise due to sampling and the discrete nature of transition events. k_{-1} was constant at $0.11 \pm 0.05\ s^{-1}$, irrespective of stimulation. After stimulation, k_2 for vesicle progression to V_2 increased from average values of $0.02 \pm 0.004\ s^{-1}$ at rest to $0.05\ s^{-1}$ and reached a first peak 5–8 s after the onset of secretion at $0.1 \pm 0.009\ s^{-1}$. k_{-2} remained unchanged at $\approx 0.03\ s^{-1}$. The spontaneous fusion rate was virtually zero such that the average lifetime $\tau(V_2)$ was given by $1/k_{-2} \approx 38$ s. After stimulation, the time course of cumulative release was non-linear. This was mostly due to depletion of pool V_2. k_3 decreased from its peak value of $0.11 \pm 0.03\ s^{-1}$ directly after stimulation to $0.05 \pm 0.03\ s^{-1}$. **B** Vesicle lifetimes in state V_1. Lifetimes were calculated as 1 over the sum of the rate constants leading away from the state. Lifetimes in state V_1, $\tau(V_1)$, scattered between a few hundred milliseconds and tens of seconds, depending on vesicle location. The average $\tau(V_1)$ did not change notably over 40 s. **C** Lifetime histogram including all data points in Fig. 3B. The time constant of the falling exponential corresponds to a mean lifetime $\overline{\tau}(V_1) \approx 3.54$ s. **D** Average lifetimes $\tau(V_2)$ are scattered over a broad range of values and decrease after stimulation. A first minimum is consistently observed 1–2 s after the onset of the stimulus with $\tau(V_2) \approx 8.5$ s. About 10–25 s after initiation of the stimulus, lifetimes are fairly constant (≈10 s) before increasing again

icle pools, using alternative biophysical approaches. Our findings emphasise the importance of the transport step that precedes immobilisation of vesicles; saturation of the secretory response was caused by the rate of vesicle supply approaching the rate of fusion.

The three-step model

The introduction of evanescent wave microscopy has made possible the direct observation of individual dye-loaded dense-core vesicles prior to exocytosis in living neuroendocrine cells (Steyer et al. 1997; Oheim et al. 1998). The trajectories of single dense-core vesicles were analysed as they approached the plasma membrane at the base of a cell illuminated by an evanescent field until they underwent exocytosis. A ~100-fold loss in 3-D mobility was observed upon approach of the vesicle to the membrane, which is interpreted as the first visualisation of the docking of a vesicle to its binding site. On the basis of fluorescence and mobility data, different functional pools of the vesicles were identified. Also examined was how stimulating secretion affects the transition rates among these states. Time-resolved studies of transitions and pool sizes together were used to arrive at estimates for the rate constants of transitions and to calculate the lifetimes of vesicles in these states.

Is V_1 well-defined based upon the available data?

The identification of states is not free from ambiguities; to identify states, the transitions between states must be fast

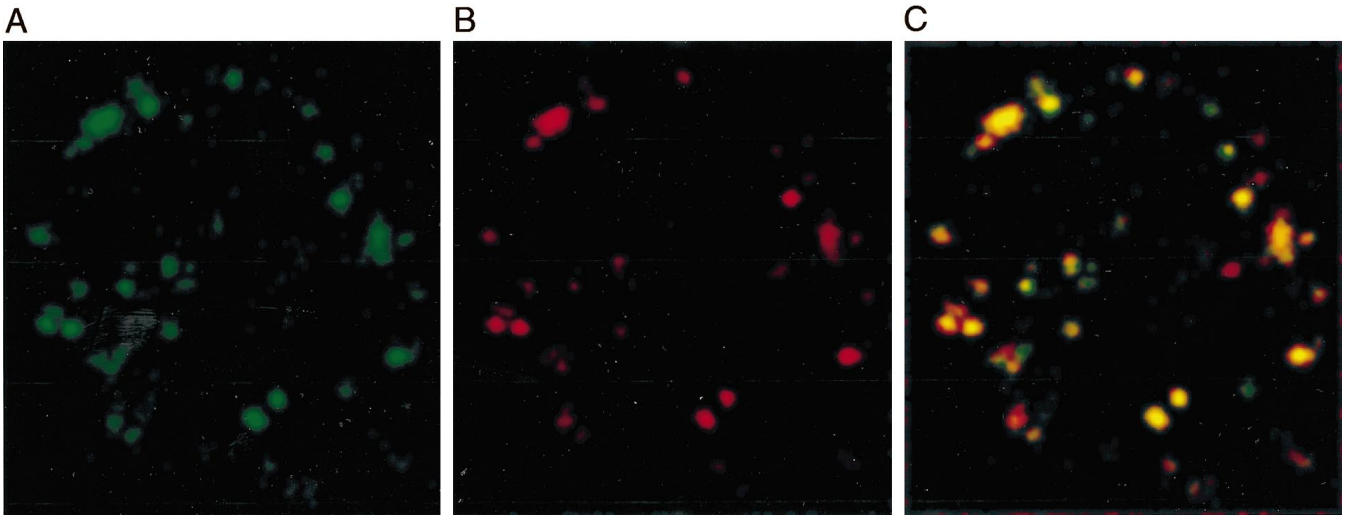

Fig. 6 A–C Sites of preferred docking and fusion. During the time before and after stimulation, vesicle activity was restricted to small patches. Once having entered the visible pool V_1, vesicles rarely displayed lateral displacements of more than 500 nm, suggesting that movement is targeted specifically to the sites of fusion. Furthermore, new vesicles often appeared repeatedly at the same location. We therefore studied the localisation of vesicle immobilisation and fusion. Co-localisation of sites of vesicle activity was studied by generating fluorescence difference images in which increases and decreases in fluorescence are represented by positive (docking or approach) or negative (fusion or withdrawal) pixel intensities. From each of the time-lapse images, the one taken two frames ahead was subtracted; thus, sites of sudden and substantial change in fluorescence were determined while excluding both immobile spots (possibly representing acidic compartments other than vesicles) and lateral jitters. Thresholding was used to distinguish between random fluctuations, on the one hand, and docking and fusion events, on the other. Subsequent integration over the stack of positive or negative difference images, respectively, yielded a cumulative picture of all regions of vesicle activity with the intensity coding for the degree of activity. The integrated images were then displayed in green and red pseudocolour. **A** *Green pixels* represent locations of increase in fluorescence intensity, i.e. vesicles appearing or approaching the membrane, while **B** *red pixels* mark sites of sudden loss of fluorescence, i.e. fusion. **C** Areas of increase and of decrease in fluorescence intensity overlap by 86%. Regions of overlap appear in *yellow pseudocolour*, and show sites of repeated vesicle approach and fusion. Note that there were some locations where single docking or fusion events occurred

compared to the lifetime of vesicles in these states. The biophysical parameters characterising these states are derived from stretches of the trajectory between transitions (see Fig. 4). In some cases, where the vesicle is rapidly changing states, it is hard to decide in which state the vesicle currently is, because the number of images between transitions is very small. The problem is thus very similar to the analysis of single-channel data and the identification of conductance and subconductance levels.

V_1 versus V_2

Unlike the identification of pool V_2, the definition of V_1 suffers from the fact that the biophysical properties of vesicles in pool V_1 are more diverse: fluctuations about the average fluorescence intensity F as well as random and directed movements are features that must be included to define the "mobile state of vesicles, farther removed from the plasma membrane". In all cells investigated, F was about half of that of the immobile near-membrane vesicles and $D^{(3)}$ was clearly distinguishable, with a factor of almost two orders of magnitude.

V_1 versus I

Whereas the differences between V_1 and V_2 were clearly resolvable, the situation is more difficult with respect to the invisible pool I. One concern might be that the "mobile pool" does not define a (steady) state but rather represents a spectrum of states from I to V_2. This view is supported by the short lifetime of vesicles in V_1 (≈3.5 s) and the diversity of ($D^{(3)}$, F) of these vesicles over time. Nevertheless, the average pair ($D^{(3)}$, F) characterising the individual vesicle was well-defined for vesicles belonging to V_1 and is well distinguished from the background intensity. Recall that vesicles were referred to as visible if their average intensity exceeded 8.5 cts above background in three consecutive frames, whereas the average value of vesicles in V_1 was ≈23.3 cts above background.

In the present study, invisible vesicles were implicitly identified as if they were a homogeneous pool, but ($D^{(3)}$, F) was not defined. Only high-resolution techniques with the ability to look deeper into the cell can resolve this problem. Using confocal microscopy, Burke et al. (1997) resolved multiple mobility groups of GFP-labelled vesicles in NGF-treated PC-12 cells. Interestingly, immobile vesicles were also present at larger distances from the plasma membrane. Another complication in the definition of V_1 is that the size of the pool of mobile vesicles that are located distant from the plasma membrane but still within a shell of a few hundred nanometers from the plasma membrane depends on d, the penetration depth of the evanescent wave. Since d is modified by the cell's footprint topography and

different cells adhere differently, the size of the mobile pool, [V_1], will be different from cell to cell, even when the calculated penetration depth is identical.

Spatial aspects of secretion control

Does locally elevated Ca^{2+} affect vesicle movement?

Previous studies using amperometry have shown regions of focal transmitter release in isolated chromaffin cells (Robinson et al. 1995). One possible explanation for this focal activity is that vesicle docking is restricted to sites where docking proteins are clustered. If the number of these sites is limited, new vesicles will be able to associate with the membrane only where a previous vesicle fusion has occurred to make the site available for further docking. These docking proteins may be physically linked to voltage-activated Ca^{2+} channels (Martin-Moutot et al. 1996; Sheng et al. 1997), where vesicles are exposed to high transients of $[Ca^{2+}]_i$ promoting rapid secretion (Llinas et al. 1981; Augustine et al. 1985; Yamada and Zucker 1992; Neher 1998). Alternatively, if vesicles are capable of docking anywhere at the plasma membrane, $[Ca^{2+}]$ gradients may help to guide vesicles to their fusion sites. In that case, vesicle mobilisation would be directed up calcium gradients, so docking and fusion would occur most commonly where the calcium concentration is highest – near the mouth of calcium channels. All vesicles would progress through the same sequence, but those nearest the calcium channels would transit through the sequence of states more rapidly. Thus, the sites of high vesicle throughput visualised by TIRFM may represent regions of docking protein and/or calcium channel clustering.

A role for the cytoskeleton?

Vesicles came to the plasma membrane unidirectionally and arrived at their future fusion sites with high specificity, leaving it unlikely that diffusion is the only component in this transport process. For all vesicles observed, approach to the plasma membrane was associated with a loss of mobility. This weakens previous hypotheses that the dissolution of a cortical actin barrier controls the progression of vesicles to the membrane and towards exocytosis. Our findings support the conclusion that the influence of the cortical actin filaments on secretion control is most likely to be one of a guide for active transport rather than of obstruction of vesicle movement. This question has become the topic of intense investigation (Wacker et al. 1998).

Conclusion

The concept of sequential maturation of vesicles through successive states has been evolving gradually, based on biochemical and biophysical studies (Bittner and Holz 1992; Heinemann et al. 1993; Thomas et al. 1993). Our findings using evanescent wave microscopy emphasise the reversibility of the transitions and provide direct measurements of the rates involved in the dynamic equilibria between the states. Previous studies have shown that Ca^{2+} may enhance the size of the readily releasable pool of vesicles (Bittner and Holz 1992; Hay and Martin 1992; Neher and Zucker 1993; von Rüden and Neher 1993). The present work corroborates and extends these studies, showing that stimulation of the cell by elevating extracellular potassium leads to selective enhancement of two forward transitions preceding the well-recognised calcium-dependent fusion step. The readily releasable pool is identified here as a subset of V_2, and it consists of vesicles that exhibit restricted mobility at the plasma membrane, most likely due to molecular attachment to the membrane. Stimulation leads to irreversible progression from V_2 to completed exocytosis. Our findings do not support the transient breakdown of a cortical actin barrier as a major element of secretion control.

Acknowledgements We thank W. Almers for critical feedback and discussions, R. Schneggenburger, C. Smith and P. Butler for the reading of and suggestions on the manuscript, F. Friedlein and M. Pilot for the preparation of the chromaffin cells and J. Ficner for technical support. The authors would like to acknowledge the support of the Nuffield Foundation, the Wellcome Trust and the Royal Society to R. H. C. This work was supported by a British Council Academic Research Collaboration (ARC) grant to W. S and R. H. C.

References

Albillos A, Dernick G, Horstmann H, Almers W, Alvarez de Toledo G, Lindau M (1997) The exocytotic event in chromaffin cells revealed by patch amperometry. Nature 389:509–512

Alvarez de Toledo G, Fernandez J (1990) Compound versus multigranular exocytosis in peritoneal mast cells. J Gen Physiol 95:397–409

Alvarez de Toledo G, Fernandez-Chacon R, Fernandez JM (1993) Release of secretory products during transient vesicle fusion. Nature 363:554–557

Ammala C, Ashcroft F, Rorsman P (1993) Calcium-independent potentiation of insulin release by cyclic AMP in single beta-cells. Nature 363:365–368

Augustine G, Charlton M, Smith S (1985) Calcium entry and transmitter release at voltage-clamped nerve terminals of squid. J Physiol (Lond) 367:163–181

Betz WJ (1970) Depression of transmitter release at the neuromuscular junction of the frog. J Physiol (Lond) 206:629

Bittner MA, Holz RW (1992) A temperature-sensitive step in exocytosis. J Biol Chem 267:16226–16229

Born M, Wolf E (1980) Principles of optics, 6th edn. Pergamon Press, Oxford

Breckenridge L, Almers W (1987) Currents through the fusion pore that forms during exocytosis of a secretory vesicle. Nature 328:814–817

Burke NV, Han W, Li D, Takimoto K, Watkins SC, Levitan ES (1997) Neuronal peptide release is limited by secretory granule mobility. Neuron 19:1095–1102

Elmqvist D, Quastel DMJ (1964) A quantitative study of end-plate potentials in isolated human muscle. J Physiol (Lond) 178:505–529

Gillis KD, Chow RH (1997) Kinetics of exocytosis in adrenal chromaffin cells. Cell Dev Biol 8:133–140

Gillis K, Misler S (1993) Enhancers of cytosolic cAMP augment depolarization-induced exocytosis from pancreatic B-cells: evidence for effects distal to Ca^{2+} entry. Pflügers Arch 424: 195–197

Gosh RN, Webb WW (1994) Automated detection and tracking of individual and clustered cell surface low density lipoprotein receptor molecules. Biophys J 66: 1301–1318

Hay JC, Martin TFJ (1992) Resolution of regulated secretion into sequential MgATP-dependent and calcium-dependent stages mediated by distinct cytosolic proteins. J Cell Biol 119: 139–151

Heinemann C, Rüden L von, Chow RH, Neher E (1993) A two-step model of secretion control in neuroendocrine cells. Pflügers Arch 424: 105–112

Horrigan FT, Bookman RJ (1994) Releasable pools and the kinetics of exocytosis in chromaffin cells. Neuron 13: 1119–1129

Llinas R, Steinberg I, Walton K (1981) Relationship between presynaptic calcium current and postsynaptic potential in squid giant synapse. Biophys J 33: 323–351

Martin-Moutot N, Charvin N, Leveque C, Sato K, Nishiki T, Kozaki S, Takahashi M, Seagar M (1996) Interaction of SNARE complexes with P/Q-type calcium channels in rat cerebellar synaptosomes. J Biol Chem 271: 6567–6570

Neher E (1998) Vesicle pools and Ca^{2+} microdomains: new tools for understanding their roles in neurotransmitter release. Neuron 20: 389–399

Neher E, Zucker R (1993) Multiple calcium-dependent processes related to secretion in bovine chromaffin cells. Neuron 10: 21–30

Oheim M, Loerke D, Stühmer W, Chow RH (1998) The last few milliseconds in the life of a secretory granule. Docking, dynamics and fusion visualized by total internal reflection fluorescence microscopy (TIRFM). Eur Biophys J 27: 83–98

Parsons TD, Coorssen JR, Horstmann A, Almers W (1995) Docked granules, the exocytic burst, and the need for ATP hydrolysis in endocrine cells. Neuron 15: 1085–1096

Robinson IM, Finnegan JM, Monck JR, Wightman RM, Fernandez JM (1995) Colocalization of calcium entry and exocytotic release sites in adrenal chromaffin cells. Proc Natl Acad Sci USA 92: 2474–2478

Rosenmund C, Stevens CF (1996) Definition of the readily releasable pool of vesicles at hippocampal synapses. Neuron 16: 1197–1207

Rüden L von, Neher E (1993) A Ca-dependent early step in the release of catecholamines from adrenal chromaffin cells. Science 262: 1061–1065

Sheng Z-H, Yokoyama CT, Catterall WA (1997) Interaction of the synprint site of N-type Ca^{2+} channels with the C2B domain of synaptotagmin I. Proc Natl Acad Sci USA 94: 5405–5410

Stevens CF, Tsujimoto T (1995) Estimates for the pool size of releasable quanta at a single central synapse and for the time required to refill the pool. Proc Natl Acad Sci USA 92: 846–849

Steyer JA, Horstmann H, Almers W (1997) Transport, docking and exocytosis of single secretory granules in live chromaffin cells. Nature 388: 474–478

Thomas P, Wong JG, Lee AK, Almers W (1993) A low affinity Ca^{2+} receptor controls the final steps in peptide secretion from pituitary melanotrophs. Neuron 11: 93–104

Wacker I, Migala A, Almers W (1998) Does the actin cortex influence sustained secretion. Abstract, C.N.R.S. Conférence Jacques Monod, La Londe les Maures, April 20–24

Yamada WM, Zucker RS (1992) Time course of transmitter release calculated from simulations of a calcium diffusion model. Biophys J 61: 671–682

Zhou Z, Neher E (1993) Mobile and immobile calcium buffer in bovine adrenal chromaffin cells. J Physiol (Lond) 469: 245–273